Short Communications

J. Synchrotron Rad. (1996). **3**, 313–315

Reticulography: a simple and sensitive technique for mapping misorientations in single crystals

A. R. Lang[a] and A. P. W. Makepeace[b]

[a]H. H. Wills Physics Laboratory, University of Bristol, Tyndall Avenue, Bristol BS8 1TL, UK, and [b]Department of Physiology, School of Medicine, University of Bristol, Bristol BS8 1TD, UK

(*Received 3 July 1996; accepted 9 August 1996*)

Interposition of a fine-scale X-ray absorbing mesh between a Laue-diffracting crystal specimen and the photographic plate recording its topographic image splits the diffracted beam into an array of individually identifiable microbeam elements. Direction differences between the microbeams in the array, which are twice the orientation differences between the crystal elements reflecting them, are measured by recording the array at two or more mesh-to-photoplate distances. Maps of misorientation vectors over the crystal lattice planes under examination can be derived from these array images by visual or digital electronic metrological procedures. Applications to two specimens widely different in diffracting properties are described. Angular size of the X-ray source is the principal instrumental factor setting misorientation detection limits, and was less than 1 arc second in this work.

Keywords: X-ray topography; crystal perfection assessment; Bragg-plane misorientation mapping.

1. Principles

Misorientation detection is a fundamental function of X-ray topography in crystal defect identification and quantification. To offset the poor incident-beam collimation provided by X-ray tube sources at practicable source-to-specimen distances, double-crystal X-ray topographic techniques were developed. They have been carried over into synchrotron radiation work, where they are widely used for crystal perfection assessment. An alternative approach with synchrotron radiation is advocated here: the detection of direction differences between spatial elements in the white-radiation diffracted beam, which are twice the orientation differences between the crystal elements reflecting them. This detection is achieved by placing a fine mesh (reticule) in the diffracted beam, and tracking the angular dispersal of the individually identifiable filamentary diffracted beams transmitted through it.

2. Experimental arrangements

Three mesh sizes have been used, mesh repeat period and mesh material being 68 μm (Ag), 42 μm (Ni) and 34 μm (Au). They were electrodeposited 'Micromesh', erstwhile product of Thorn-EMI Electron Tubes Limited. The ratios of mesh aperture area to mesh unit cell area were ~0.4, and mesh thicknesses were ~5 μm. For the dominant wavelengths recorded, absorption by the

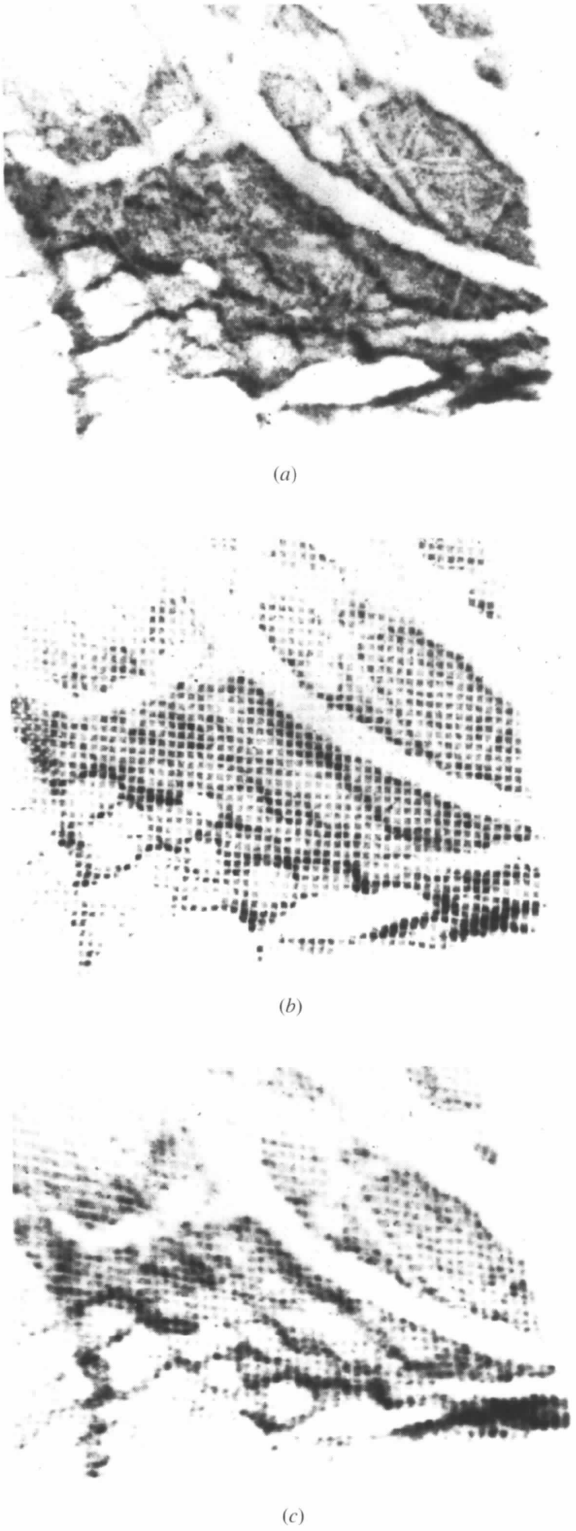

(*a*)

(*b*)

(*c*)

Figure 1
Images of the (001)-orientation surface of a Cu single crystal, 004 symmetrical reflection, $2\theta_B = 135°$, $\lambda = 1.67$ Å. Field width 3.75 mm. Recorded on Agfa-Gevaert Strukturix D2 film. (*a*) Standard surface reflection X-ray topograph, distance P from specimen to film (or plate) = 70 mm. (*b*) Reticulograph, 68 μm mesh, $P = 70$ mm, $M = 5$ mm. (*c*) Reticulograph, 68 μm mesh, $P = 86.5$ mm, $M = 21.5$ mm.

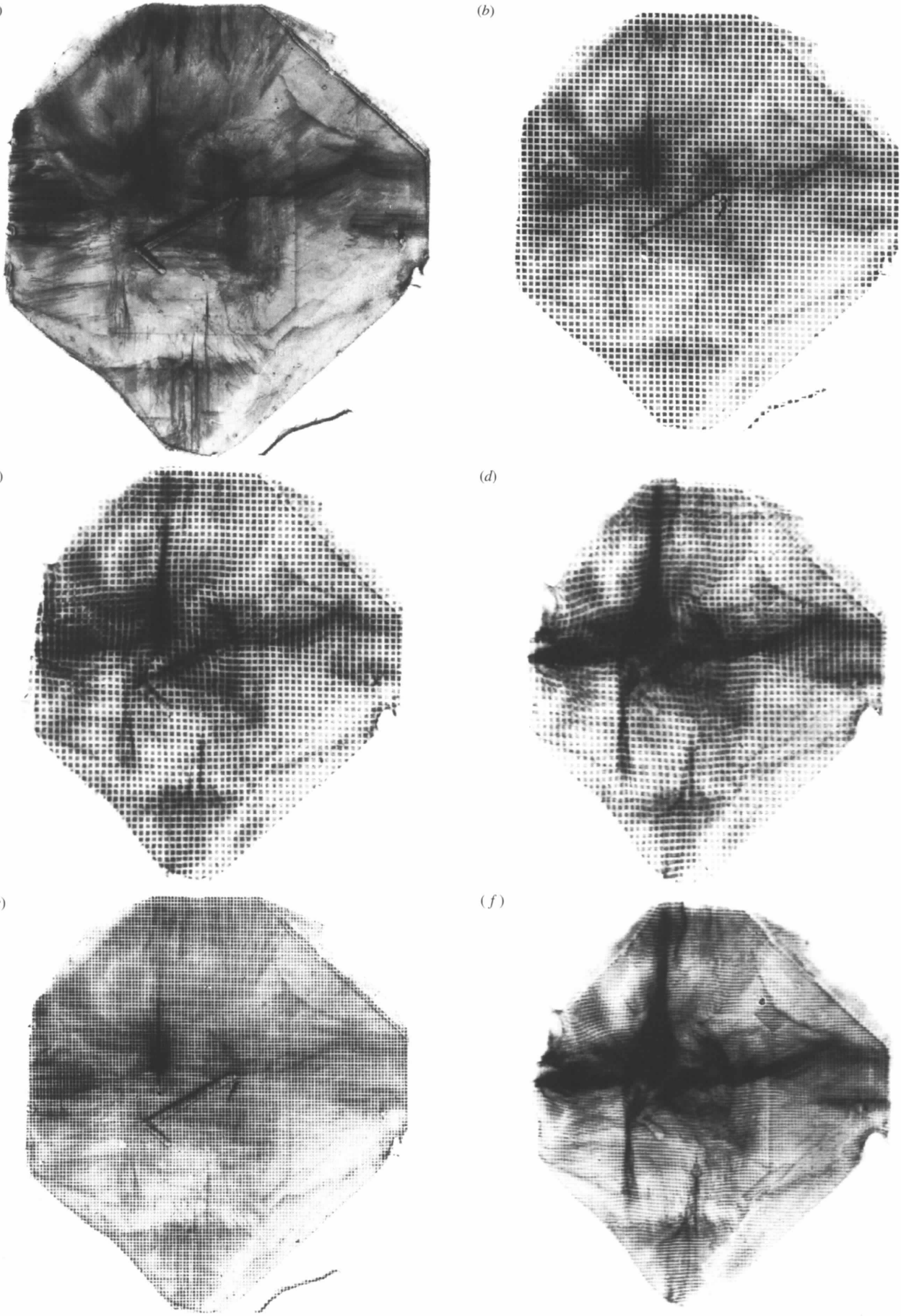
(a)
(b)
(c)
(d)
(e)
(f)

Au, Ag and Ni mesh bars was near total, strong and light, respectively. A lightly absorbing mesh renders inessential 'mesh-free' reference topographic images. However, for measuring relative displacements of mesh-cell images as a function of distance M between mesh and photographic plate, from which cell-to-cell $2\theta_B$ differences (and hence lattice orientation differences) are determined, the high-contrast images given by Au and Ag meshes were preferred both in visual and electronic metrological procedures.

Working at Station 7.6 at Daresbury, 80 m from the tangent point, with source FWHM 0.23 mm vertically and 2.3 mm horizontally, the incidence angular range in the vertical diffraction plane is ~ 3 μrad (~ 0.6 arc seconds).

3. Applications

Two very different specimens are shown here. The first is a (001)-orientation electropolished slice of melt-grown single-crystal copper. The back-reflection topograph of the 20 mm-diameter slice's central area, Fig. 1(*a*), reveals both intrinsic and processing-induced defects: the mosaic structure produces the ripple-like pattern dominant in the lower part of the image, whereas surface scratches, both coarse and fine, appear as curving blank lines prominent in the upper part of the image. Fig. 1(*b*), a recticulograph with minimum M, already shows some mesh-image irregularity, which becomes more pronounced in Fig. 1(*c*). The mesh image recorded with M = 40 mm (not exhibited) was significantly less sharp than in Fig. 1(*c*); it showed the intrinsic angular reflecting range from individual area elements to be ~ 250 μrad, about four times the 'perfect-crystal' reflecting range for λ = 1.67 Å calculated from dynamical diffraction theory. Increases in the irregular displacements of mesh shadows as M increases indicate that random misorientations occurring on a cell-to-cell spatial scale are also ~ 250 μrad in magnitude.

Patterns produced by a large synthetic diamond (Fig. 2) contrast greatly with those of Fig. 1. The diamond is patently more perfect; its reticulograph perturbations at M = 260 mm (Fig. 2*c*) are not much greater than those of the copper at M = 5 mm (Fig. 1*b*). Now one can take advantage of the finer image subdivision afforded by the 34 μm mesh (Figs. 2*e* and 2*f*). When M = 635 mm, resolution of vertical bars is clearly limited by X-ray source horizontal dimensions. However, the sharpness of horizontal bar images in both Figs. 2(*d*) and 2(*f*) demonstrates that in several regions the angular range of reflection by substantial groups of cells is 20 μrad or less, comparable with the calculated perfect-crystal value, 14 μrad. The surface imaged is that at which the seed crystal (originally nearer the observer) was cut away. The roughly square [001]-direction growth sector occupying the surface centre is flanked by octahedral and other cube growth sectors, the configuration of growth sectors and dislocations broadly resembling that in another similarly cut specimen (Lang, 1994). An artefact is the figure '7' laser-inscribed near the surface centre. Its downstroke is composed of two parallel strokes ~ 75 μm apart. They have tilted bodily a shallow strip of diamond lying between them so that it produces the image strip seen lower right of the main image in Figs. 2(*a*), 2(*b*) and 2(*e*). Representative of natural features interpretable *via* reticulography are arrays of dislocations running vertically and generating vertical bands of high intensity, most evident at higher P. They produce folds in the mesh pattern, incipient at M = 260 mm (Fig. 2*c*) and well developed at M = 635 mm (Fig. 2*d*), thereby identifying their tilt-boundary action in producing lattice 'kinks' concave towards the observer.

Figure 2
(See opposite.) Images of the $(00\bar{1})$-orientation surface (cut, but damage-free) of a synthetic diamond of cubo-octahedral habit. Direction [110] vertical, $00\bar{4}$ symmetrical reflection, $2\theta_B = 135°$, λ = 1.65 Å. Crystal width 3.9 mm. The direction of view, being rotated 22.5° from $[00\bar{1}]$ towards [110], brings into oblique view the side crystal facets (100), upper left, and (010), upper right, seen weakly by radiation transmitted from the $(00\bar{1})$ surface. Recorded on Ilford Nuclear Emulsion, 25 μm thick. (*a*) Surface reflection topograph, P = 65 mm. (*b*)–(*f*) Reticulographs: (*b*)–(*d*) 68 μm mesh, (*e*) and (*f*) 34 μm mesh. (*b*) P = 65 mm, M = 10 mm. (*c*) P = 315 mm, M = 260 mm. (*d*) P = 690 mm, M = 635 mm. (*e*) P = 65 mm, M = 10 mm. (*f*) P = 690 mm, M = 635 mm.

4. Digital pattern analysis

Reticulographs are eminently suitable for this procedure. Fig. 2(*c*) was treated as follows. An optical microscope with low-power objective projected an image of the reticulograph directly into a CCD camera, using only the microscope centre field so as to avoid distortion. The magnification provided ~ 20 pixels per 68 μm, fully avoiding aliasing. Used with a 512 by 512 pixels frame-grabber, a digital reference grid composed of 1 pixel-width lines was created from a scanned mesh radiograph and was electronically superimposed on the stored reticulograph image. On print-outs, displacements of reticulograph cells relative to the reference mesh were easily measurable by eye to 1/20 cell period. With M = 260 mm this corresponds to lattice orientation changes of only ~ 6 μrad.

5. Prospects

Versatility resides in the wide range of sensitivity, simply controlled by choice of M distances. Using $2\theta_B$ values high enough to avoid major asterism, reticulographs show equally well both orthogonal components of misorientation vectors. By contrast, double-crystal topograph sequences show only one. For the great majority of crystal characterization tasks, from growth defect studies to monochromator assessment, reticulography can replace double-crystal topography at synchrotron X-ray sources. When double-crystal topography is needed for lattice parameter measurements, prior reticulographic examination is advisable to select specimen regions sufficiently misorientation-free.

The authors thank the Director and Staff, Synchrotron Radiation Department, Daresbury Laboratory, for provision of experimental facilities.

References

Lang, A. R. (1994). *J. Appl. Cryst.* **27**, 988–1001.